Acid−Base Interactions and Secondary Structures of Poly-L-Lysine Probed by ^{15}N and ^{13}C Solid State NMR and *Ab initio* Model Calculations

Alexandra Dos,[‡] Volkmar Schimming,[‡] Sergio Tosoni,[§] and Hans-Heinrich Limbach*,[‡]

Institut für Chemie und Biochemie, Freie Universität Berlin, Takustrasse 3, D-14195 Berlin, Germany, and Dipartimento Chimica IFM, University of Torino, Via P. Giuria 7, 10125 Torino, Italy

Received: July 24, 2008; Revised Manuscript Received: September 18, 2008

The interactions of the ^{15}N-labeled amino groups of dry solid poly-L-lysine (PLL) with various halogen and oxygen acids HX and the relation to the secondary structure have been studied using solid-state ^{15}N and ^{13}C CPMAS NMR spectroscopy (CP = cross polarization and MAS = magic angle spinning). For comparison, ^{15}N NMR spectra of an aqueous solution of PLL were measured as a function of pH. In order to understand the effects of protonation and hydration on the ^{15}N chemical shifts of the amino groups, DFT and chemical shielding calculations were performed on isolated methylamine−acid complexes and on periodic halide clusters of the type $(CH_3NH_3^+X^-)_n$. The combined experimental and computational results reveal low-field shifts of the amino nitrogens upon interaction with the oxygen acids HX = HF, H_2SO_4, CH_3COOH, $(CH_3)_2POOH$, H_3PO_4, HNO_3, and internal carbamic acid formed by reaction of the amino groups with gaseous CO_2. Evidence is obtained that only hydrogen-bonded species of the type $(Lys-NH_2\cdots H-X)_n$ are formed in the absence of water. ^{15}N chemical shifts are maximum when H is located in the hydrogen bond center and then decrease again upon full protonation, as found for aqueous solution at low pH. By contrast, halogen acids interact in a different way. They form internal salts of the type $(Lys-NH_3^+X^-)_n$ via the interaction of many acid−base pairs. This salt formation is possible only in the β-sheet conformation. By contrast, the formation of hydrogen-bonded complexes can occur both in β-sheet domains as well as in α-helical domains. The ^{15}N chemical shifts of the protonated ammonium groups increase when the size of the interacting halogen anions is increased from chloride to iodide and when the number of the interacting anions is increased. Thus, the observed high-field ^{15}N shift of ammonium groups upon hydration is the consequence of replacing interacting halogen atoms by oxygen atoms.

Introduction

Poly-L-lysine (PLL) constitutes an important basic poly amino acid (Scheme 1) which has numerous applications in material and pharmaceutical science. It also constitutes an interesting polyelectrolyte as the amino groups are easily protonated. Using a combination of high-resolution ^{15}N solid-state NMR and quantum chemical calculations, we have obtained novel insights into the type of acid−base interactions of PLL which depend on the chemical structure of the acid and the water content; both have an influence on the secondary structure.

It has well been established that PLL can adopt different secondary structures such as the β-pleated sheet and the α-helix, as illustrated in Figure 1, or a coil. X-ray diffraction studies of solid fibers of PLL × HCl and PLL × HBr containing several water molecules per residue revealed a β-pleated sheet structure with a high degree of crystallinity,[1,2] as illustrated in Figure 1a. The conformation of the side chains, the geometries of the ammonium halide ion pairs, and the position of the water molecules could not be determined. On the basis of the distances between the β-pleated sheets, which varied between 15 and 17 Å depending on the water content, a salt structure model illustrated schematically in Figure 1b was derived. It was supposed that all three protons of the alkylammonium groups are in contact with three halides and vice versa.[2] If water was removed, amorphous[2] or glassy[3] structures were observed, corroborated by ^{13}C solid-state NMR.[4,5] At higher degrees of hydration, hexagonally crystallizing α-helices were formed (Figure 1d),[1,2] which can be also formed in the presence of monohydrogen phosphate and water.[6] On the other hand, excessive hydration destroys the long-range order and produces a random coil.[1,2] By contrast, dry PLL lyophilized at high pH consists of a mixture of β-pleated sheets and α-helices, as revealed by ^{13}C solid-state NMR[7] and IR[8] spectroscopic studies.

SCHEME 1: Chemical Structure of Poly-L-lysine Labeled with ^{15}N in the ε Position (PLL)

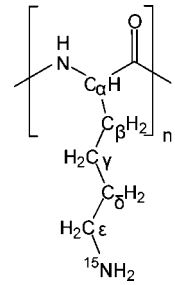

poly-L-lysine (PLL)

In aqueous solution, the secondary structures of poly-L-lysine have been studied using various spectroscopic techniques, ranging from optical methods to NMR.[9] As mentioned above, at low pH, a random coil conformation is formed. Raman optical activity (ROA)[10] studies showed that this structure exhibits regions corresponding to α-helices, β-pleated sheets, and left-

* To whom correspondence should be addressed. E-mail: limbach@chemie.fu-berlin.de.
‡ Freie Universität Berlin.
§ University of Torino.

10.1021/jp806551u CCC: $40.75
Published on Web 11/14/2008

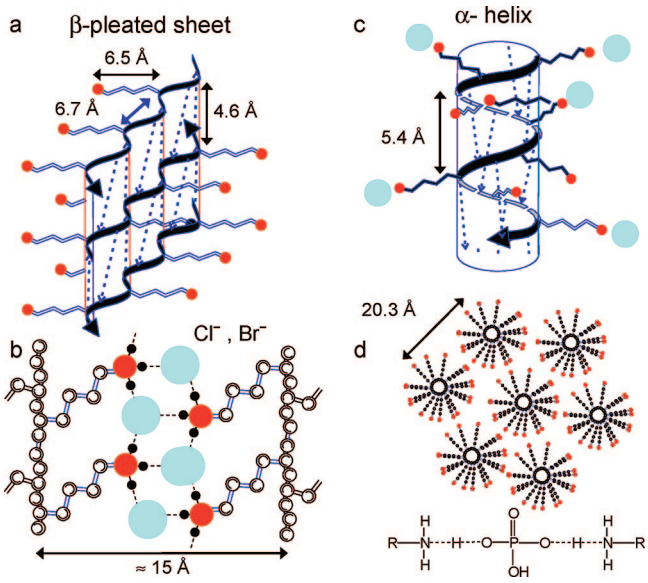

Figure 1. Secondary structures of poly-L-lysine. (a) β-pleated sheet of PLL × HX according to ref 1 (X = Cl) and ref 2 (X = Br). The side chain length was taken from the crystal structure of L-lysine monohydrochloride dihydrate.[56] (b) A salt-like ammonium halide interaction model according to ref 2. (c) α-Helical conformation (schematically). (d) Hexagonally arranged α-helices of wet PLL × H_3PO_4 according to ref 6. The chain−chain distance is approximately 20 Å.

handed helices. At pH 9−11, a transformation to an α-helix is observed by ^{13}C NMR.[11] Heating the basic solution leads again to the formation of β-pleated sheets, as revealed by ESR and NMR,[12] optical rotatory dispersion measurements,[13] and Raman spectroscopy.[14] IR measurements showed that the secondary structure is also influenced by the chain length.[15,16] According to Scheraga, the β-pleated sheet structure is favored by hydrophobic interactions between the side chains by which the entropy of the surrounding water is increased.[17]

In summary, the focus of previous research has been to monitor changes of the secondary structures of PLL induced by changes of pH, hydration, the type of counterion, and so forth; however, because of the lack of suitable spectroscopic probes, there is only little knowledge of the interactions of the ammonium side groups with their surroundings. To our knowledge, the only IR tool to monitor protonated ammonium side groups of PLL is an NH stretching band at 3030 cm^{-1} found by Rozenberg et al.[18] in the case of dry solid PLL × HBr. Other bands gave indications about the secondary structure which depend on the sample preparation.

For a long time, it has been known that ^{15}N chemical shifts of alkylammonium groups are diagnostic for their protonation state, but a detailed knowledge of the dependence on the hydrogen bond geometries is still lacking. A natural abundance ^{15}N NMR study of Hull et al.[19] of PLL in water at different pHs revealed a high-field shift of the terminal nitrogen atom at high pH, in agreement with previous findings for simple amines.[20] Unfortunately, the intrinsic chemical shift of the "free" amino group of PPL in water could not be determined. Evidence was obtained that the deprotonation is accompanied by a change of the secondary structure from random coil to α-helix, but the question remained open whether ^{15}N NMR chemical shifts are directly influenced by the secondary structure or only indirectly via the preference for a certain protonation state. This question is difficult to solve by liquid-state NMR as the ammonium groups of lysine side chains are solvated in aqueous solution and as their ^{15}N chemical shifts represent averages over the protonated and nonprotonated hydrated states.

The situation is, however, different in the case of the dry solid state, where proton transfer may be slow and where intrinsic ^{15}N chemical shifts obtained by ^{15}N CPMAS NMR (CP = cross polarization, MAS = magic angle spinning) can probe the acid−base interactions of lysine side chains. This tool has not yet been exploited to date. Some time ago, some of us showed that in this state, the free amino groups of a solid ornithine amino bolaamphiphile lyophilized at high pH can form carbamate with gaseous CO_2 in a similar way as in aqueous solution;[21] the same reaction was observed for solid poly-L-lysine.[21] In the course of these studies, we noticed a ^{15}N chemical shift difference of more than 20 ppm between nonprotonated amino groups and the corresponding protonated hydrochloride. A similar deprotonation shift was observed recently for the naturally occurring ε-PLL, where the side chain amino group forms the peptide bonds.[22] This difference is much larger than expected for a simple protonation-deprotonation in water.[20] In other words, when alkylammonium or ammonium[23] is transferred from a solid halide salt environment to aqueous solution, the nitrogen is shielded strongly, although the protonation state remains the same. For example, a hydration shift of about −12 ppm has been observed for ammonium chloride.[24] The effect is also present, although smaller, in the case of aqueous solution. Hansen et al.[25] have shown that ammonium groups are deshielded at low pH when the concentration of halide counterions is increased. The low-field shifts increase from chloride to iodide, whereas no effect occurs for nitrate. This effect was clearly attributed to a partial replacement of hydrate water by the counteranion. However, the reasons for both deprotonation as well as hydration shifts of ammonium groups are still unexplored and have, therefore, not widely been used in the solid-state NMR of proteins.

Therefore, we undertook the present solid-state ^{15}N NMR study of dry solid $^{15}N_\varepsilon$ poly-L-lysine (PLL, Scheme 1) lyophilized in the presence of different acids and explored the effects of acid−base interactions on the ^{15}N chemical shifts. We included the effects of gaseous CO_2, which produces carbamic acid in the dry solid state with deprotonated amine side chains.[21] Whenever it seemed useful, we performed ^{13}C solid-state NMR measurements in order to analyze the secondary structures according to the strategy of Kricheldorf.[7] ^{13}C solid state NMR can also give information about the mobility of lysine side chains induced by hydration,[4,26] but studies of the effects of pH variation and water content on the acid−base properties of PLL were beyond the scope of the present study, a task which we will perform in the near future. Only for comparison of the solid-state results with those of aqueous solution did we measure the ^{15}N chemical shifts of PLL in water as a function of pH. The effects of changing pH and of adding water are currently studied and will be published in subsequent papers.

In order to confirm the diagnostic value of the ^{15}N chemical shifts, we have performed DFT calculations of methylamine as a model base interacting with different acids, both for the gas phase as well as for selected halogen acids also in the solid state, and have subsequently calculated the associated ^{15}N shieldings.

This paper is organized as follows. In the Experimental Section, the details of the sample synthesis and preparation, of the NMR studies, and of the calculations are reported. Then, we describe the results of the liquid- and solid-state NMR experiments on poly-L-lysine interacting with different acids. Finally, the results are discussed.

Experimental Section

Synthesis of $^{15}N_\epsilon$-poly-L-lysine Hydrochloride. The PLL used in this study was enriched to about 50% with ^{15}N in the ε position of the side chain. For that purpose, a mixture of $^{15}N_\epsilon$-L-lysine hydrochloride (98% ^{15}N, Campro Scientific GmbH) and the unlabeled material was polymerized as follows. In the first step, labeled and unlabeled N_ε-carbobenzoxy-L-lysine was prepared by reaction of benzyl chloroformiate[27] with the copper chelate complex of L-lysine.[28] In the second step, N_ε-carbobenzoxy-L-lysine-N_α-carboxyanhydrid (NCA) was prepared by reaction with phosgene.[29] Unlabeled and labeled NCA were then mixed together in dioxane, where N_ε-carbobenzoxy-protected poly-L-lysine was produced with sodium methoxide as the initiator.[29] The protection group was then removed with 33% HBr in acetic acid,[30] adding a saturated aqueous solution of $NaHCO_3$ until a pH of 7 was obtained, and treatment with ether, which produced an aqueous solution of PLL × HBr. In the next step, an aqueous solution of PLL × HCl was obtained by dialysis against dilute hydrochloric acid using membrane tubes with a molecular weight cutoff of 1000 and 2000 Daltons (Type Zellu Trans, V-Series, Carl Roth Company, Karlsruhe, Germany). The solution was then lyophilized to yield solid PLL × HCl. The molecular weight distribution had been determined previously for the N_ε-carbobenzoxy-protected poly-L-lysine by size exclusion chromatography (Biogel P-10, Bio Rad, excl. limit 20000) and/or gel chromatography (Sephacryl S-500HR, Sigma excl. limit 40000−20000000). The results showed that the final product PLL × HCl exhibited a molecular weight of 160000 ± 40000 Daltons, corresponding to 1000 ± 250 monomers in the polypeptide.

Sample Preparation. ***Liquid Samples.*** Liquid samples were prepared by dissolving about 5 mg of PLL × HCl in about 0.7 mL of water, leading to 0.04 M solutions with respect to lysine monomers. The pH was adjusted with small quantities of HCl or NaOH in the same solvent. The samples with pH > 8 were frozen and warmed to 283 K only shortly before the NMR experiments in order to prevent gel formation.

Lyophilized Dry Samples of PLL × HX. Solid samples of PLL × HX were prepared by dialysis of PLL × HCl against dilute aqueous solutions of the desired acid. The solutions were then set to the desired pH by adding small quantities of a sodium hydroxide solution or the desired acid.

In the case of the acid- and ion-free sample, an aqueous solution of PLL × HCl was desalted using an anion exchange resin (Bio Rad AGI-X2, 200−400 mesh, OH^- form or Dowex 2 × 8−200, 100−200 mesh, OH^- form, prepared from the Cl^- forms), which increased the pH to about 12. Then, the sample was lyophilized and dried. The sample of PLL × dimethylphosphinic acid was prepared from the solution of the acid- and ion-free sample by adding small amounts of an aqueous solution of the acid.

During the operations described above, contact with air was minimized in order to avoid carbamate formation of PLL. It occurs in water around pH 10 as well as in the dry solid state in acid-free dry PLL.[21] Therefore, all solutions as well as the bidistilled water were degassed in vacuo and were consequently flushed with argon.

The lyophilized samples were transferred into rotors and consecutively dried further inside of the uncapped rotor at room temperature in vacuo at a pressure below 10^{-6} mbar. On average, the samples were kept at this pressure for 16−20 h and then flushed with dry argon. The rotors were closed with Teflon sealing caps and measured by NMR. Using ^1H MAS NMR, no liquid-type water could be detected in these samples.

NMR Spectroscopy. All solid-state measurements were carried out on a Varian Infinity Plus 600 spectrometer at a ^{15}N resonance frequency of 60.8 MHz and a ^{13}C resonance frequency of 150.88 MHz. All measurements were performed at ambient temperature. Spinning speeds between 5 and 10 kHz were used. The ^{13}C NMR spectra were calibrated to TSP (sodium salt of 3-(trimethylsilyl)-propionic acid-d_4). The ^{15}N solid-state NMR spectra were referenced to solid NH_4Cl using glycine (100% ^{15}N and ^{13}C enriched) as an intermediate reference.

The liquid-state ^{15}N NMR spectra of PLL in H_2O as a function of pH were measured using a Bruker AMX 500 spectrometer (500.13 MHz for ^1H, 50.68 MHz for ^{15}N). Standard inverse ^1H decoupled ^{15}N NMR spectra were recorded with a recycle time of 3 s. The magnetic field lock was established using D_2O contained in a capillary inside of the NMR tube.

In order to reference the ^{15}N chemical shifts of PLL in water, we proceeded as described previously.[31] For that purpose, we recorded the ^{15}N spectrum of neat nitromethane containing a capillary with D_2O, that is, under the same ^2H field locking conditions as in the case of the aqueous PLL solutions. In order to convert the ^{15}N chemical shifts from the nitromethane scale into the solid external solid $^{15}NH_4Cl$ scale, the relation $\delta(CH_3{}^{15}NO_2, \text{liq.}) = \delta(^{15}NH_4Cl, \text{solid}) - 341.168$ ppm was used.[24]

Ab Initio and Chemical Shift Calculations. The calculations of methylamine with different counterions in the gas phase were performed at the B3LYP/6-31g(d,p) level[32] using Gaussian 03.[33] This program also allowed us to calculate the GIAO nuclear magnetic shielding values of all nuclei, but only the ^{15}N values were analyzed. Solid-state calculations were performed with PW91/6-31g(d,p)[34,35] using CRYSTAL06.[36] The choice of the basis set for solid-state calculations is, in general, not trivial. The CRYSTAL06 webpage (http://www.crystal.unito.it) hosts a database from where we took the basis sets that have been used in the present work. For C and N, the 6-21G* basis set has been adopted.[37] H electrons are described with a 3-1G* basis set.[38] As far as the counterions are concerned, all-electrons basis sets are used for fluorine (7-311G)[39] and chlorine (86-311G),[40] while for bromine, a HAYWLC-31 set is adopted, where the core electrons are described using the Hay and Wadt large effective core pseudopotentials.[41]

All graphical manipulations necessary to create and visualize the CRYSTAL input and output files were made with MOLDRAW.[42] In order to let the structure relax, both internal coordinates and cell parameters have been optimized; therefore, also the distance of hydrogen bonds that are formally split between two adjacent cells is in equilibrium.

Results

pH Dependence of $^{15}N_\epsilon$-poly-L-lysine in Aqueous Solution. In a first stage of this study, we measured the ^{15}N NMR spectra of $^{15}N_\varepsilon$-poly-L-lysine in water as a function of pH, at a concentration of 0.04 M with respect to the lysine amine/ammonium groups. The pH was adjusted by adding small quantities of aqueous NaOH or HCl. The results are shown in Figure 2. The signals obtained below pH 7 and above pH 13 are sharp and exhibit line widths of less than 10 Hz. Between pH 9.2 and 11.4, line widths on the order of 30 Hz are observed, arising from the onset of gel formation, which previously prevented the establishing of a full pH titration curve.[19] As this process is slower at lower temperatures, we performed the measurements shown in Figure 2 at 283 K. The lower temperature and the ^{15}N enrichment gave us then enough time to take the spectra.

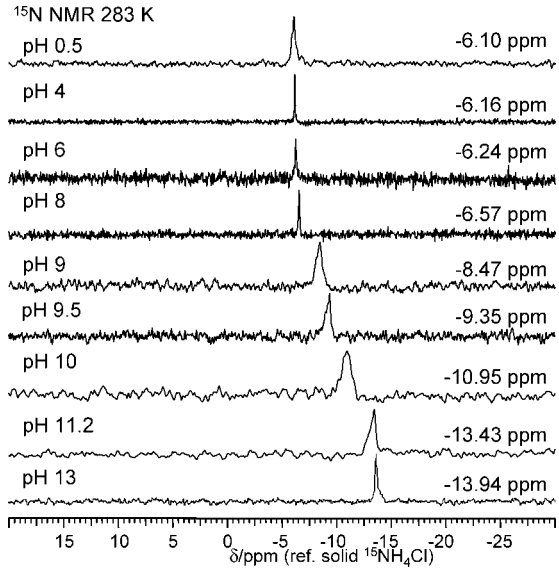

Figure 2. ^{15}N NMR signals of PLL-$^{15}N_\varepsilon$ in water as a function of pH obtained at 50.68 MHz and 283 K.

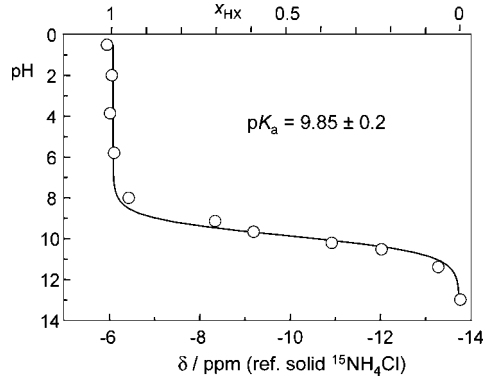

Figure 3. Henderson−Hasselbalch plot of the ^{15}N NMR chemical shifts of PLL-$^{15}N_\varepsilon$ in water.

In Figure 3 are plotted the chemical shifts δ as a function of pH. The solid line was calculated using the NMR version of the Henderson−Hasselbalch equation[43]

$$\delta = \delta_{NH3+} + (\delta_{NH3+} - \delta_{NH2})\frac{10^{pH-pK_a}}{1 + 10^{pH-pK_a}} \qquad (1)$$

The parameters of eq 1 were obtained using a nonlinear least-squares fitting routine. $\delta_{NH3+} = -6.1$ ppm represents the ^{15}N chemical shift of the protonated amino groups and $\delta_{NH2} = -13.95$ ppm the value of the deprotonated amino groups. Their pK_a value was found to be 9.85 ± 0.20. We note that a single pK_a value was sufficient to describe the data. In other words, in aqueous solution, the acid−base properties of the amino side chains are independent of each other within the margin of error of our experiments.

^{15}N Solid-State NMR Studies of N_ε-poly-L-lysine with Various Acids. ***Carbamic Acid Formed by Reaction with Gaseous CO_2.*** The ^{15}N CPMAS NMR spectrum of an ion- and acid-free dry sample of PLL lyophilized at pH 12 is depicted in Figure 4a. The deprotonated amino group labeled as base "B" gives rise to a relatively sharp Lorentzian line centered around −16.5 ppm with respect to external solid NH_4Cl.

When the PLL solution at pH 12 was exposed to air for 1 day, the pH had dropped to about 5.5, indicating the incorporation of CO_2.[21] Lyophilization at this pH and subsequent drying gave then the ^{15}N CPMAS NMR spectrum depicted in Figure 4b, containing two new lines A1 and A2 at 42 and 48 ppm. However, when the solution was exposed to air only for about half of a day and the pH was readjusted to 11.4 before lyophilization, the spectrum shown in Figure 4c was obtained in which signal A1 was absent.

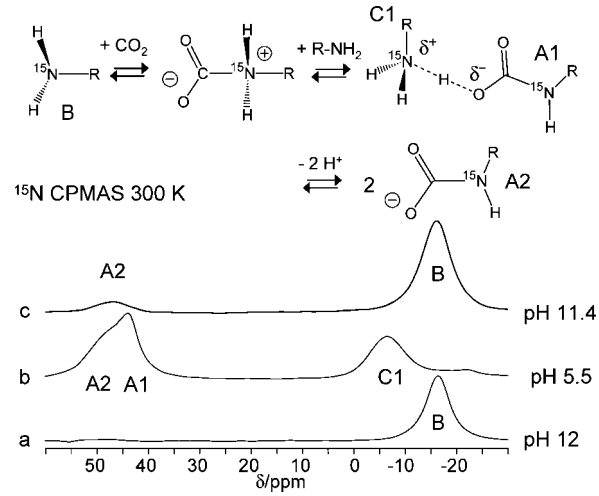

Figure 4. Room-temperature ^{15}N CPMAS NMR spectra of dry solid PLL. (a) After lyophilization and drying of an acid- and ion-free PLL sample of pH 12. (b) After exposure of the solution for 1 day to air, resulting in a drop of pH to 5.5, and lyophilization and drying without adding base. (c) After exposure of the solution for half of a day to air, readjustment of the pH to 11.4, and lyophilization and drying. The assignment of the amide signal A has been shown previously via dipolar $^{13}C-^{15}N$ couplings using REDOR techniques.[21] For further explanation, see the text.

As was shown previously using dipolar REDOR techniques,[21] the new signals in Figure 4b and c around 50 ppm arise from carbamate groups formed by reaction of the free amino groups with CO_2. This reaction does not only take place in solution but also in the solid state.[21] Therefore, the carbamate-free sample of Figure 4a had been kept under argon. Once the rotor was closed with caps, no carbamate formation could be observed any more.

We assign signal A2 to a sodium carbamate species as A1 does not appear in the spectrum of the sample of Figure 4c, which was lyophilized at high pH. The presence of the sodium carbamate species does not affect the signal of the remaining free amino groups B. By contrast, the sample of Figure 4b contained obviously carbamic acid species interacting with remaining amino groups, shifting them to −6.5 ppm. At first sight, it is tempting to assign this shift to the formation of alkylammonium as found in water at low pH (Figure 2), but the sample did not contain any water. Therefore, we assign this shift to the hydrogen-bonded acid−base complex in Figure 4; this complex is labeled as "C1", where C stands for complex and 1 for the number of interacting amino groups per acid. This interpretation will be further supported in the next section. A similar shift had been observed previously for a carbamic acid containing ornithine amino bolaamphiphile, but we had not recognized the origin of this shift.[21] We can then assign signal A1 to the hydrogen-bonded complex. These results show that when studying PLL in the absence of acids, care has to be taken to avoid carbamate formation.

Added Acids. Figure 5 shows the ^{15}N CPMAS NMR spectra of poly-L-lysine lyophilized in the absence and presence of different acids as well as the liquid-state NMR spectra at high

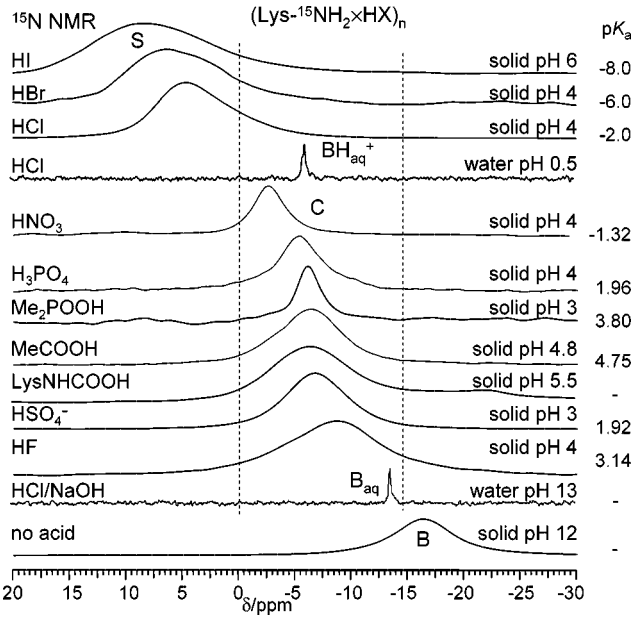

Figure 5. Room-temperature ^{15}N CPMAS spectra of dry PLL and PLL × HX. For comparison, the ^{15}N NMR spectra of PLL at pH 0.5 and 13 are included. For further explanation, see the text.

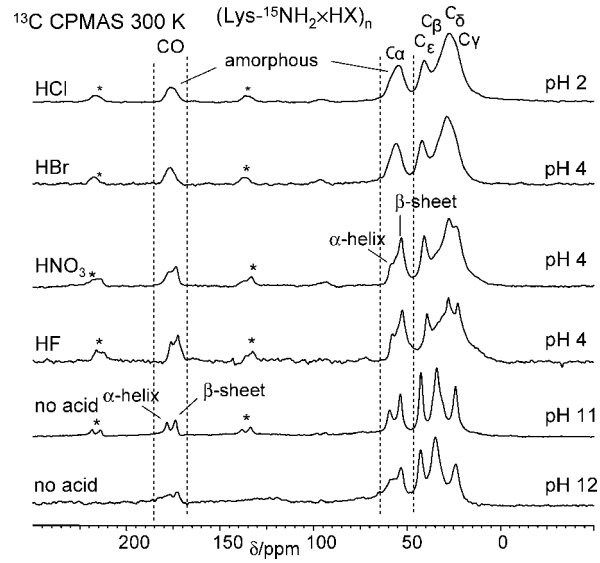

Figure 6. ^{13}C CPMAS spectra of PLL × HX and of PLL lyophilized at different pH values indicated on the right side. The asterisks indicate rotational side bands.

and low pH. Generally, lyophilization was performed at pH values around 5, as indicated on the right side of Figure 5. As these values are well below the pK_a value of the amino groups, it was ensured that all amino groups of PLL were protonated with the deprotonated acid as the counteranion. On the other hand, we tried to avoid the presence of more than one acid molecule per monomer unit of PLL. Removal of water during the lyophilization process brings the ammonium and counterions into hydrogen bond contact formally described as $RNH_2 \times HX$. There is one exception, i.e. sulfuric acid where the interacting acid HX is $NaHSO_4$.

As mentioned above, the free amino groups B of dry PLL resonate at around −16.5 ppm. In the presence of proton donors, low-field shifts are observed, which depend on the type of the acid. The smallest signal shift is observed for PLL in water at high pH. Larger values are observed in the solid state for HF and various oxygen acids. The largest low-field shift is observed for HNO_3 to about −3 ppm. We assign these species to hydrogen-bonded complexes C. By contrast, in water at pH 0.5, where the alkylammonium groups are fully protonated, the signal is shifted again to a higher field, that is, −6.1 ppm.

The other halogen acids behave in a different way. Here, very broad signals are observed above 0 ppm. A monotonous deshielding occurs when the size of the halogen anion is increased from chloride via bromide to iodide. We label this region as "S", which stands for salt formation, as discussed later. This behavior is in strong contrast to the behavior of HF. In conclusion, the $^{15}N_\varepsilon$ chemical shifts are affected by the absence or the presence of the acids in a different way.

^{13}C Solid-State NMR Studies of N_ε-poly-L-lysine with Various Acids. Figure 6 depicts ^{13}C CPMAS NMR spectra of dry PLL in contact with hydrogen halides and with HNO_3 lyophilized at low pH. For comparison, the spectra of nonprotonated PLL lyophilized at pH 11 and 12 are included.

In the latter samples, we observe two lines for the carbonyl group at 176 and 172 ppm and two lines at 58 and 52 ppm for the C_α carbon. These signals have been assigned by Kricheldorf et al.[7] and are of a high diagnostic value; the lower-field bands correspond to α-helices and the high-field lines to β-pleated sheets, as illustrated in Figure 1. Thus, our nonprotonated PLL sample corresponds to a mixture of both secondary structures.

We obtained similar results for PLL interacting with HF and with HNO_3, although the resolution of the lines was somewhat reduced. However, only single Lorentzian ^{15}N lines were observed for these samples, as illustrated in Figure 5. This indicates that the nitrogen chemical shifts are diagnostic only for the protonation and hydrogen-bonded state of the amino groups; thus, they do not probe directly the secondary structure adopted but only indirectly if a change of the secondary structure leads to a different protonation or hydrogen-bonded state. On the other hand, as discussed below, two different secondary structures may prefer different protonation states, which could then lead to different ^{15}N chemical shifts, as discussed later.

In contrast, the hydrochloride and hydrobromide exhibit nonresolved broad lines for both ^{13}C environments. These results are in agreement with previous observations,[4,5] and with the finding by X-ray diffraction[1,2] that dry PLL × HCl and PLL × HBr exhibit β-pleated sheet structures containing so many defects that the crystalline solids become amorphous when water is entirely removed.

DFT Calculations of Geometries and of ^{15}N Chemical Shielding Values of Methylamine−Acid Complexes. In order to assist the interpretation of the ^{15}N NMR data of PLL, we have performed DFT calculations for isolated methylamine−acid complexes. Some important distances of the optimized geometries are assembled in Table 1, as well as the calculated chemical shielding values. In addition, we have included the experimental ^{15}N chemical shifts of PLL.

In Figure 7, the calculated equilibrium structures of methylamine 1:1 complexes with the proton donors HX = H_2O, HF, HCl, and HBr are depicted. For comparison, we include also the complex with three water molecules and one with a single water and a single HCl molecule. When the acidity of HX is increased, the distance H···X increases, and the distance N···H decreases. The proton donor power of water increases when it is part of a longer chain[44] or if an HCl molecule is added, leading to a shortening of the H···N distances. However, in all cases besides HBr, the H···X distances are smaller than the N···H distances, that is, in the gas phase, no acid besides HBr is able to protonate methylamine. This result is similar to the one ob-

TABLE 1: Hydrogen Bond Distances, ^{15}N Chemical Shielding Values, and ^{15}N Chemical Shifts of Methylamine-Acid Model Complexes and of Dry Poly-L-lysine Interacting with Different Acids[a]

	R = CH_3						R = PLL		
system	$\sigma(^{15}N)$	r_{NH1}	r_{H1X1}	r_{NX1}	r_{NH2}	r_{NH3}	$\delta(^{15}N)$	r_{NH1}[b]	r_{H1X1}[b]
$RNH_2 \times HBr$	214.4	1.271	1.720	2.983	1.019	1.019	6.17		
$RNH_2 \times HCl$	224.6	1.553	1.400	2.952	1.018	1.018	4.2		
$RNH_2 \times HNO_3$	232.9	1.583	1.047	2.630	1.019	1.018	−2.87	1.35	1.15
$RNH_2 \times H_3PO_4$	233.7	1.615	1.036	2.630	1.023	1.017	−5.3	1.47	1.09
$RNH_2 \times R_2POOH$	227.9	1.669	1.023	2.667	1.024	1.017	−6.0	1.50	1.07
$RNH_2 \times RCOOH$	229.5	1.706	1.016	2.703	1.021	1.017	−6.1	1.52	1.07
$RNH_2 \times RNHCOOH$	231.2	1.695	1.014	2.689	1.022	1.017	−6.5	1.55	1.06
$RNH_2 \times NaHSO_4$	236.0	1.621	1.032	2.644	1.017	1.021	−6.71	1.54	1.06
$RNH_2 \times HF$	238.7	1.677	0.959	2.600	1.017	1.017	−9.2	1.57	1.00
$RNH_3^+F^-$		1.073	1.569	2.635	1.070	1.070			
$RNH_3^+Cl^-$	216.0	1.055	2.110	3.150	1.055	1.055	4	1.04	2.2
$RNH_3^+Br^-$	215.7	1.050	2.330	3.350	1.050	1.050	6	1.035	2.4
$RNH_3^+I^-$							9		
RNH_2	244.1				1.017	1.017	−16.5		
$RNH_2 \times H_2O$	240.4	1.925	0.981	2.855	1.017	1.017	−14		
RNH_3^+	235.2	1.097			1.093	1.093			
$RNH_3^+ \times H_2O$	233.3	1.062	1.641	2.697	1.024	1.024			
$RNH_3^+ \times 2H_2O$	233.6	1.049	1.715	2.757	1.022	1.049			
			1.712	2.754					
$RNH_3^+ \times 3H_2O$	235.5	1.041	1.770	2.807	1.041	1.041	−6.1	1.07	1.6
			1.771	2.809					
			1.765	2.800					
$RNH_2 \times H_2O \times HCl$	238.3	1.734	1.006	2.726	1.018	1.018			
$RNH_2 \times 3\ H_2O$	239.6	1.739	1.007	2.736	1.018	1.030			
				2.950					

[a] Distances in Å, and chemical shielding values $\sigma(^{15}N)$ and chemical shift values $\delta(^{15}N)$ in ppm. Reference: solid $^{15}NH_4Cl$. [b] Extrapolated values according to the correlation line in Figure 13a.

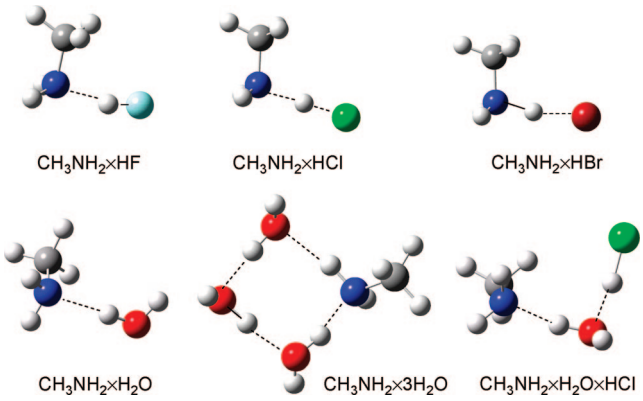

Figure 7. Calculated equilibrium structures of methylamine complexes with halogen acids and water. For further explanations, see the text.

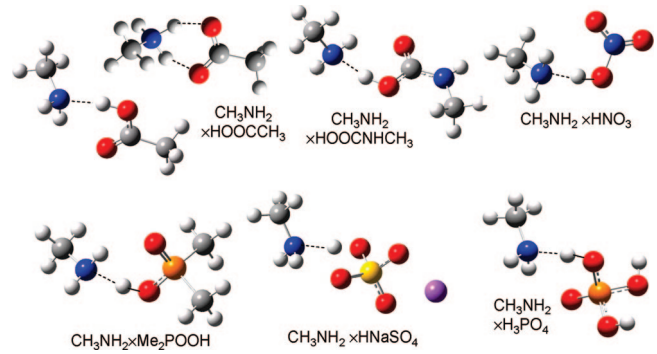

Figure 8. Calculated equilibrium structures of methylamine complexes with various oxygen acids. For further explanations, see the text.

tained for ammonia acid complexes which protonate the base only in the presence of strong electric fields.[45]

The situation does not change significantly in the case of the oxygen acid complexes depicted in Figure 8. In almost all cases, 1:1 hydrogen bonds involving the acid as the proton donor are formed; weaker hydrogen bond contacts are established between the "free" NH groups and the additional oxygen atoms of the donor. The situation can change if H is transferred to nitrogen, producing zwitterionic states which do not correspond to the stationary state in the gas phase. As shown for the complex with acetic acid, in this case, two hydrogen bonds can be formed involving two NH groups of methylammonium and two oxygen atoms of the acetate anion.

In Figure 9 are depicted geometries of protonated methylamine complexes with one to three molecules of water. We did not add an anion as, in this case, the proton is transferred back from nitrogen to the anion, as was found in the complex with one water and one HCl molecule depicted in Figure 7. Thus, methylammonium in water needs to be stabilized by a larger number of water molecules.

Another possibility which we had to consider is salt structures where methylammonium forms three hydrogen bonds to three different counterions and where each counterion forms three hydrogen bonds to three different methylammonium groups, as suggested for PLL × HBr by Suwalsky et al.[2] on the basis of X-ray powder diffraction patterns (Figure 1b). We have calculated corresponding layered salt structures under periodic boundary conditions for the methylammonium halides MAH^+F^-, MAH^+Cl^-, and MAH^+Br^-. The results are included in Table 1. All halides form a similar structure to the MAH^+Cl^- depicted in Figure 10, with NH distances of 1.073, 1.055Å, and 1.050 Å and H···X distances of 1.569, 2.110, and 2.330 Å. The increase of the latter reflects the size of the anion.

In the next step, we calculated the absolute isotropic shielding values σ_N of the nitrogen atom of all methylamine species using the calculated geometries as input parameters. In the case of the layered salt structures, we calculated the values for the

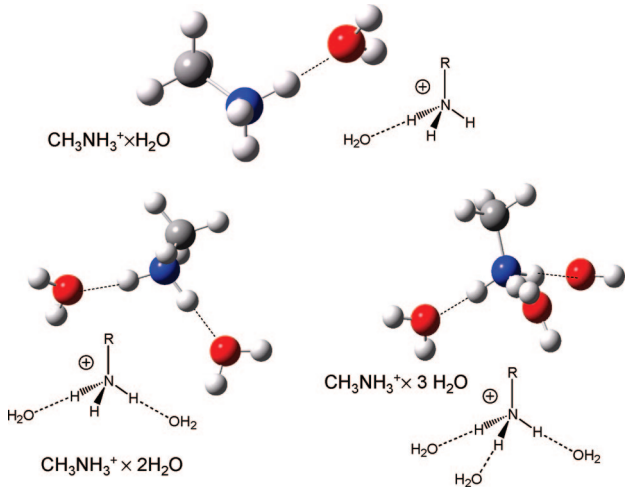

Figure 9. Calculated equilibrium structures of methylammonium complexes with water. For further explanations, see the text.

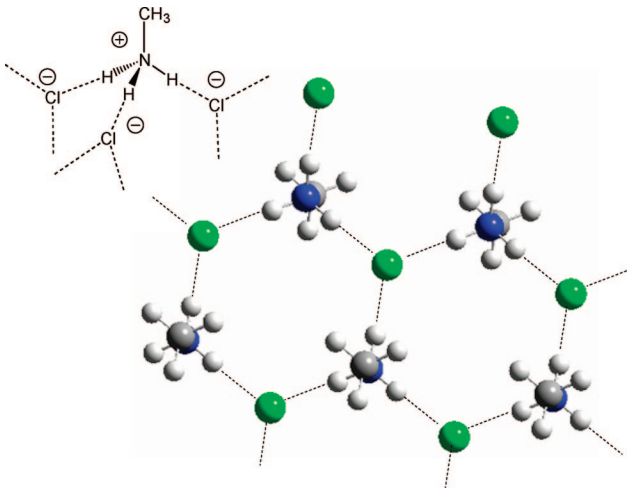

Figure 10. Calculated equilibrium structure of a methylammonium chloride layer. For further explanations, see the text.

central nitrogen in a neutral cluster of nine ammonium halide units exhibiting the geometry of the periodic layer. The results are included in Table 1. We note that the Gaussian03 program calculates the isotropic and anistotropic chemical shielding values of all nuclei contained in the molecule of interest. However, the detailed analysis of the chemical shielding tensors as well as how they are located in the molecular frames was beyond the scope of this study.

Hydrogen Bond Correlation Analysis. In order to discuss the calculated data, we use recent findings,[46] of hydrogen bond correlations between the two distances $r_1 = r_{AH}$ and $r_2 = r_{HX}$ of a given hydrogen-bonded system A−H···X or between the natural hydrogen bond coordinates q_1 and q_2 defined as

$$q_1 = \frac{1}{2}(r_1 - r_2) \qquad q_2 = r_1 + r_2 \tag{2}$$

In the case of a linear hydrogen bond, q_1 corresponds directly to the distance of the proton with respect to the hydrogen bond center and q_2 to the heavy-atom A···X distance. According to the valence bond order concept of Pauling, Brown, and Dunitz et al.,[47] one can associate to the two bonds of a hydrogen bridge bond valences given by

$$p_1 = \exp\{-(r_1 - r_1^\circ)/b_1\} \qquad \text{and} \qquad p_2 = \exp\{-(r_2 - r_2^\circ)/b_2\} \tag{3}$$

where r_1° and r_2° represent the equilibrium distances in the fictive free diatomic units AH and HX and b_1 and b_2 describe bond order decays with increasing bond distances. As the valence of hydrogen is unity, it follows that

$$p_1 + p_2 = \exp\{-(r_1 - r_1^\circ)/b_1\} + \exp\{-(r_2 - r_2^\circ)/b_2\} = 1 \tag{4}$$

Thus, both distances r_1 and r_2 depend on each other. Using eq 4, it is possible to express r_1 as a function of r_2 or q_1 as a function of q_2. The validity of this equation has been demonstrated in a number of cases.[45,46,48−50] An empirical correction for quantum zero-point vibrational effects (QZPVE) was introduced recently, which needs to be taken into account when discussing H/D isotope effects on hydrogen bond geometries.[51,52] The parameters used to calculate the solid lines are included in Table 2.

Figure 11a contains a graph of the hydrogen bond coordinate q_2 as a function of the proton coordinate q_1. For comparison, in Figure 11b are plotted the distances r_{HX} as a function of r_{NH}. The data points refer to the calculated equilibrium structures of the hydrogen-bonded complexes listed in Table 1. For the halogenides also, the results from the solid-state calculations are included. The solid lines were calculated using eqs 2−4 and the parameters assembled in Table 2, which were taken from previous work. The data points, which will be discussed later in more detail, are well located on these curves.

In Figure 12, we have plotted the calculated isotropic chemical shielding constants σ_N of the amino nitrogen atoms interacting with different acids as a function of the distances r_{NH}. The small filled circles refer to nonequilibrium geometries listed in Table S1 of the Supporting Information. The larger filled squares refer to equilibrium geometries listed in Table 1. The nonequilibrium geometries were used to derive the solid correlation curves, which were calculated using the equation[51,52]

$$\sigma(\underline{N}HX) = \sigma(\underline{N}H)^\circ p_{NH} + \sigma(\underline{N})^\circ p_{HX} + 4\sigma^*(\underline{N}HX) p_{NH} p_{HX}{}^m \tag{5}$$

Here, $\sigma(\underline{N}H)^\circ$ represents the shielding constant of isolated protonated methylamine $CH_3NH_3^+$, and $\sigma(\underline{N})^\circ$ is the value of the unprotonated isolated methylamine CH_3NH_2. These values are independent of the acid as the acid or their anions are far away in the isolated methylamine and methylammonium. In other words, $\sigma(\underline{N}H)^\circ - \sigma(\underline{N})^\circ$ represents the protonation shift. Thus, these values were kept constant for all correlation lines in Figure 12. The $\sigma^*(\underline{N}HX)$ represents the term giving rise to the difference in the correlation curves of Figure 12; it represents the excess shift of the nitrogen for the case where the two valence bond orders $p_{NH} = p_{HX} = 0.5$. The values of σ^* are listed in Table 3. They vary strongly with the heavy atom of the proton donor and somewhat also with the structure of the donor. The exponent m in eq 5 is a fitting parameter included in Table 3.

We note that the excess term increases with the size of the heavy bridge atom of the proton donor. This leads to substantial low-field shifts in the case of the $CH_3NH_2 \times HCl$ and $CH_3NH_2 \times HBr$ complexes. Maximum shifts, that is, shielding minima,

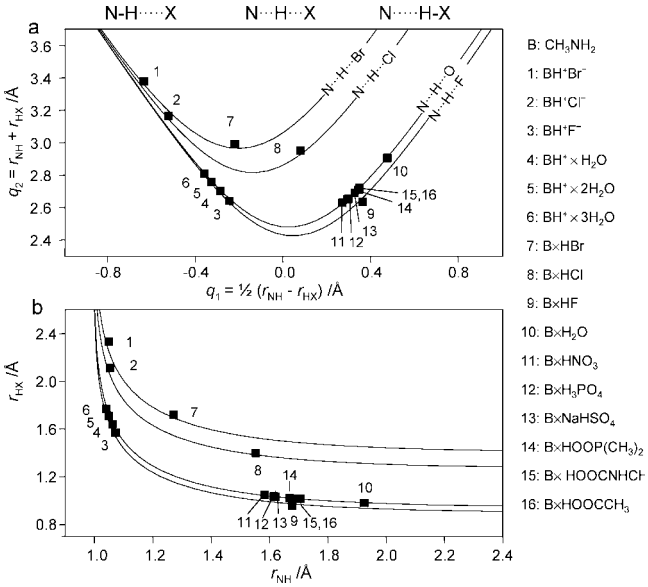

Figure 11. Hydrogen bond correlation of calculated equilibrium structures of methylammonium halides and of methylamine−acid complexes. (a) Heavy-atom coordinate q_2 as a function of the hydrogen bond coordinate q_1. (b) r_{HX} as a function of r_{NH}. The solid correlation lines were calculated as described in the text.

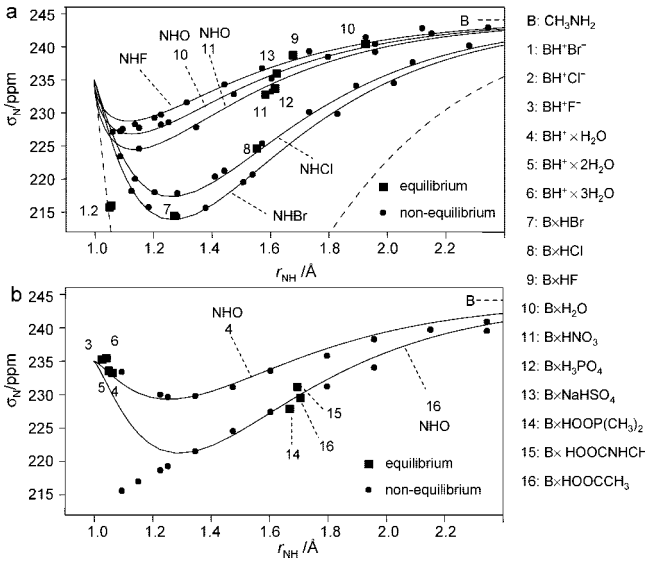

Figure 12. Calculated ^{15}N chemical shielding constants of isolated $CH_3NH_2 \times HX$ complexes as a function of the calculated NH distance. (a) HX = HF, H_2O, HNO_3, HCl, HBr. (b) HX = H_3O^+, CH_3COOH. The small circles refer to nonequilibrium geometries corresponding to the correlation curves of Figure 11. The large squares refer to the calculated equilibrium geometries.

TABLE 2: Parameters of the Geometric Hydrogen Bond Correlation of $RNH_2 \times HX$ (eq 4)

system	b_{NH}/Å	$r_{NH}°$/Å	b_{HO}/Å	$r_{HO}°$/Å
NHO[51,52]	0.385	0.992	0.371	0.942
NHF[49]	0.385	0.992	0.36	0.897
NHCl[45]	0.385	0.992	0.382	1.27
NHBr[45]	0.385	0.992	0.399	1.407

are obtained in the region of the shortest hydrogen bonds. The shielding values of the crystalline salts $CH_3NH_3^+Cl^-$ and $CH_3NH_3^+Br^-$ are close to the minima found for the hydrogen-bonded complexes. This effect can be explained with the dashed correlation line, calculated with a larger value of $\Delta\sigma$, which we associate with the presence of three halide anions around

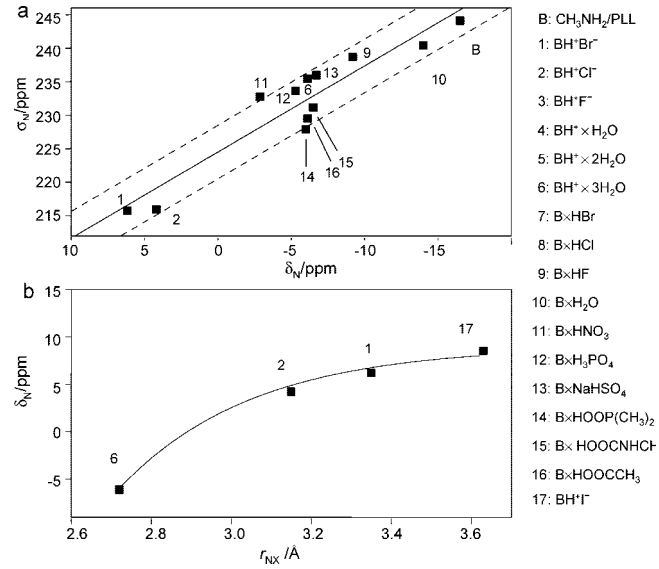

Figure 13. (a) Calculated ^{15}N chemical shielding constants of isolated $CH_3NH_2 \times HX$ complexes as a function of the experimental ^{15}N chemical shifts of PLL interacting with the same acids. (b) Experimental ^{15}N chemical shifts of PLL × HX, HX = H_2O, HCl, HBr, and HI as a function of the calculated N···X distances.

TABLE 3: Parameters of the NMR Hydrogen Bond Correlation of $RNH_2 \times HX$

system	σ(N)°/ppm	σ(NH)°/ppm	σ*(NHX)/ppm	m
$RNH_2 \times H_2O$	244	235	8.0	0.6
$RNH_2 \times HNO_3$	244	235	9.8	0.6
$RNH_2 \times H_3O^+(H_2O)_2$	244	235	12.5	1.3
$RNH_2 \times RCOOH$	244	235	22.5	1.3
$RNH_2 \times HF$	244	235	6.3	0.6
$RNH_2 \times HCl$	244	235	23.8	1.1
$RNH_2 \times HBr$	244	235	27.5	1.1
$(RNH_2 \times HCl)_n$	244	235	37.5	1.1
$(RNH_2 \times HBr)_n$	244	235	37.5	1.1

ammonium in the crystalline state in contrast to a single halide in the 1:1 complexes. As the concerted shift of H from nitrogen to the halogen atom or the increase of the nitrogen-halide distances destroys the crystal, the dashed line is valid only around the data points 1 and 2, and was, therefore, dashed.

The values of σ* are similar for fluorine and simple oxygen acids such as water. Larger values are observed for HNO_3, H_3O^+, and CH_3COOH. For a better visualization, the latter two curves were placed in a separate graph, Figure 12b. These curves describe already very well the calculated data of the different acids. Therefore, we did not calculate further nonequilibrium geometries for the other acid−base complexes.

We note that eq 5 can describe the methylamine−acetic acid complexes only at larger NH distances. At shorter distances, the shielding values are smaller than predicted by the solid correlation line. We associate this effect with the formation of two hydrogen bonds in the zwitterionic methylammonium−acetate complex when H has been transferred to nitrogen (Figure 8).

We have plotted in Figure 13a the calculated isotropic nitrogen chemical shielding values σ_N of the calculated equilibrium structures of $CH_3NH_3 \times HX$ as a function of the nitrogen chemical shifts δ_N (reference solid ammonium chloride) of the corresponding PLL samples. We obtain a fairly good linear correlation corresponding to the equation

$$\sigma_N = -1.285 \times \delta_N + 224.5 \text{ ppm} \quad (6)$$

We have, however, added the dashed lines in Figure 13a in order to estimate the margin of error of this correlation. In the next step, we have calculated the isotropic shielding values of the different PLL × HX samples using eq 6, starting from their experimental chemical shifts. Then, we varied the corresponding N···H distances in such a way that the estimated shielding values satisfied the correlation lines of Figure 12. Finally, from the NH distances, the corresponding H···X distances were obtained using eq 4. The results are included in the last two columns of Table 1. The deviations of these values from those calculated for methylamine complexes provide an estimate of the margins of error of the true hydrogen bond geometries. In comparison with the calculated values of the methylamine complexes, this analysis indicates shorter N···H distances and longer H···X distances for PLL.

Finally, in Figure 13b, we have prepared a graph of the experimental ^{15}N chemical shifts of PLL in water at low pH as a measure for $RNH_3^+(H_2O)_3$ and for solid PLL × HCl, PLL × HBr, and PLL × HI as a function of the N···X distances (Table 1) calculated for the corresponding methylammonium complexes. As this distance was not available for iodide, we used for that purpose the distance of 3.622 Å reported for ammonium iodide. We observe an exponential relation with increasing N···X distances caused by the increase of the size of the halide ion.

Discussion

Interaction of Amino Acid Side Chains with Added Acids. *NMR Spectroscopy.* The main findings of this study are the following. ^{15}N CPMAS NMR of dry lyophilized solid poly-L-lysine reveals that the isotropic ^{15}N NMR chemical shifts of the side chain amino groups exhibit interesting variations depending on the absence or presence of interacting acids and depending on their chemical nature. In principle, the lyophilization leads to a reduction of the local dielectric constant and hence to the formation of neutral acid-base complexes which may exhibit a zwitterionic structure; an interaction of many of these complexes can lead to a local salt formation. Moreover, although a direct influence of the chemical shifts by the secondary structure, that is, β-pleated sheets, α-helical domains, or amorphous regions, was not observed, there is an interplay between the secondary structures and the acid−base interactions of the amino groups, as was established by ^{13}C CPMAS NMR.

Three typical spectral areas were observed (Figure 5). Free amino groups produced in dry PLL by lyophilization at high pH resonate at high field at around −16.5 ppm. Under this condition, PLL consists of a mixture of β-pleated sheets and α-helical domains. However, the ^{15}N chemical shifts are the same for both domains. The situation is depicted schematically in Figure 14a.

When the amino groups are allowed to interact with HF or with various oxygen acids, ^{15}N low-field shifts are produced, which are discussed in terms of hydrogen-bonded complexes C of the type $(Lys-NH_2\cdots H-X)_n$. Again, ^{13}C NMR reveals a mixture of β-pleated sheets and α-helical domains. The largest ^{15}N shift is observed for HNO_3 and the smallest shift for HF. The ^{15}N signals are relatively narrow and Lorentzian. This might be the result of either well-defined environments or of local anisotropic reorientations.

Some samples exhibit clearly broader lines, which most probably stem from a distribution of chemical shielding values arising from a variation of hydrogen bond geometries. Particularly, broad bands are observed for acetic acid and for the internal carbamic acid. The latter can be formed in the dry solid state[21] or in aqueous solution at high pH before lyophilization (Figure 4). This leads to a substantial drop of pH. Lyophilization produces then carbamic acid residues hydrogen bonded to remaining amino groups, unless the pH is increased again before lyophilization.

The observed ^{15}N downfield shifts may be associated with increasing H···X and decreasing N···H distances when the acidity is increased. This behavior is expected for hydrogen-bonded complexes which exhibit little interaction with each other, for example, if these complexes are isolated or separated. Similar shifts, although upfield instead of downfield, have been observed for pyridine acid−base complexes and have been related to the N···H distances in a quantitative way. A scenario corresponding to the hydrogen-bonded complexes discussed is depicted schematically in Figure 14b.

By contrast, much larger downfield ^{15}N shifts are observed in the case of added HCl, HBr, and HI (Figure 5, top). The dry powders give rise to broad lines in area S, which stands for salt formation of the type $(Lys-NH_3^+X^-)_n$. For $X = Cl^-$ and Br^-, powder X-ray diffraction studies have provided evidence for such a local β-pleated sheet salt structure (Figure 1b) in the presence of a small number of water molecules.[1,2] The long-range order of the salt structure disappears when all water is removed,[2] which is consistent with our findings of broad ^{15}N signals for these halides and for iodine (Figure 5). Another broadening mechanism could arise from a quenching of local molecular motions by the salt formation. As salt formation consists of a positive charge on nitrogen and a negative charge on the halide, it follows that the nitrogen protonation state corresponds to "ammonium" groups with short NH distances of about 1 Å. The situation is depicted schematically in Figure 14c.

We note that such salt structures can only be formed if many hydrogen-bonded complexes can interact with each other. A well-known case is ammonium chloride, formed by aggregation of many hydrogen-bonded ammonia halide complexes, in which H is located in the case of the isolated complexes on chlorine rather than on nitrogen.[45] As a consequence, it seems that in the α-helical domains, the side chains interacting with an acid cannot come close enough in a sufficient number to form a local salt structure.

On the other hand, why do HF and the oxygen acids not form salt structures? For the halogen acids, it has been established theoretically that electric fields are necessary in the isolated complexes with ammonia in order to transfer the proton of the acid to nitrogen.[45] Such fields can be produced by neighboring dipoles, in particular, a second hydrogen-bonded complex. The field produced decreases with the cubic distance to the neighboring dipole. Now, the electric field necessary for proton transfer to nitrogen is particularly large in the case of HF, much smaller for HCl, and even smaller for HBr. Thus, PLL even in the β-sheet conformation does not allow the $Lys-NH_2\cdots H-F$ dipoles to come close enough as required for salt formation, in contrast to the other halogen acids.

A further feature of the halide anions is that they can form three or more hydrogen bonds to proton donors in almost all directions of space. This enables one to establish the salt network with the ammonium side chains in PLL (Figure 14c). By contrast, oxygen acids contain several oxygen atoms in a molecular frame, which allows them to form hydrogen bonds only in specific orientations, which may prevent the

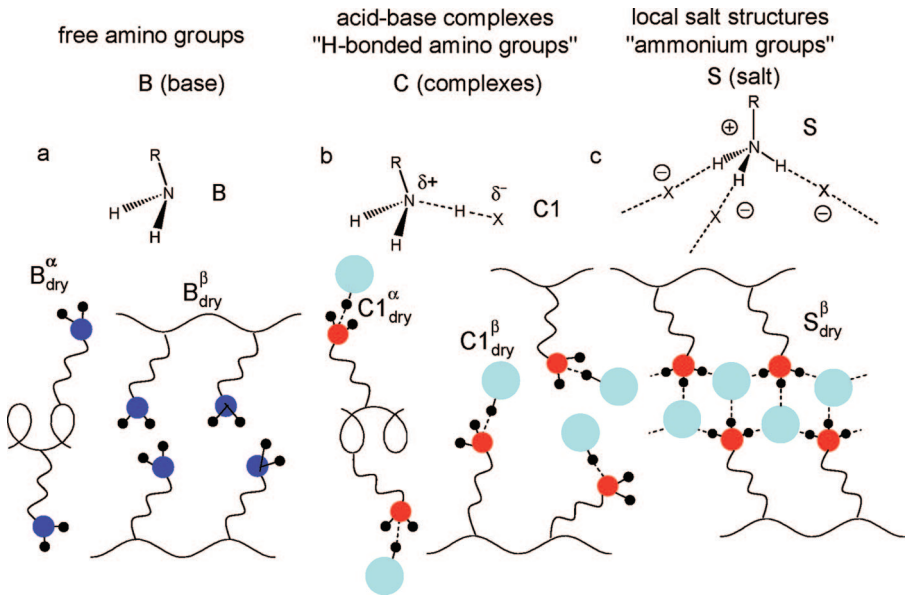

Figure 14. Scenario of acid−base interactions in dry PLL.

salt formation by a mismatch between many amino side chains and oxygen acid anions.

Computational-Assisted ^{15}N Chemical Shift Analysis: Hydration versus Protonation Shift of Amine/Ammonium Groups. One of our goals had been also to understand the two different factors, protonation and hydration, which influence the ^{15}N chemical shifts of amino groups in chemical and biological systems. This problem was solved by the ab initio DFT model calculations of isolated methylamine−HX complexes as well as that of methylammonium halides under periodic boundary conditions, coupled to subsequent calculations of the isotropic ^{15}N chemical shielding values and a subsequent hydrogen bond correlation analysis.

The calculated structures of the isolated hydrogen-bonded complexes of methylamine with proton donors (Figures 8 and 9) indicate the formation of single H bonds in the equilibrium configurations. In the case of acetic acid, a proton was transferred to nitrogen into a configuration which might be stable only in the presence of a strong electric field. In this case, two hydrogen bonds between two protons of the resulting methylammonium group to the two oxygen atoms of acetate are formed. By contrast, in the presence of several water molecules and in the case of the halide salts, all three protons were involved in hydrogen bonds (Figures 9 and 10).

As illustrated in Figure 11, the calculated distances r_{NH} and r_{HX} of all methylamine−acid species are correlated with each other, where the dependence is governed by the type of heavy atom of the bridge. The solid lines in Figure 11 were not adapted to the calculated data points but taken from previous analyses. It was confirmed that simple correlation lines without correction for quantum zero point-vibrational effects can describe the data calculated for the equilibrium geometries of hydrogen-bonded systems.[45,51,55] A new finding of Figure 11 is that also the hydrogen bond geometries of ammonium groups in salt structures are located on the same correlation lines valid for the isolated complexes where only one of the three NH units is involved in the hydrogen bond.

Figure 12 shows the calculated ^{15}N shielding values as a function of the distance r_{NH}. The small circles refer to non-equilibrium geometries and the large squares to equilibrium geometries. The solid and dashed correlation lines were calculated using the formalism described above. Before we discuss the findings of Figure 12, let us first mention that the computed chemical shielding anisotropies (Supporting Information) are partially responsible for the features of the calculated curves in Figure 12. However, as the determination of the chemical shielding tensors of PLL was beyond the scope of this study, we will discuss neither the values of the chemical shielding anisotropies nor the arrangement of the corresponding tensor in the molecular frame; for that purpose, further experimental and theoretical work will be necessary.

When H is located on the acid and far from nitrogen, the ^{15}N chemical shielding value is the same for all acids HX, that is, 244 ppm, typical for isolated methylamine. When a hydrogen bond is formed to nitrogen, that is, the distance r_{HX} is increased and r_{NH} is decreased, the ^{15}N shielding value first decreases. This decrease strongly depends on the type of the bridge atom of the acid. It is much stronger in the case of HCl and HBr as compared to HF or HOR; the latter two behave in a similar way. At a given value of r_{NH}, however, a minimum is reached, and the shielding values are increased again. All curves join at the smallest possible distance r_{NH}, corresponding to the isolated methylammonium ion, exhibiting a shielding of 235 ppm. We note that this value is about 5 ppm smaller than the corresponding value calculated for the ammonium ion.[25] Thus, the methyl group gives rise to a low-field shift of about 5 ppm, which is in agreement with the experiment.[20] The calculated ^{15}N chemical shielding value of the hydrated methylammonium ion is only slightly smaller than the one of the isolated ion (Figure 12b, Table 1), as was noted before for the ammonium ion.[25]

The curves in Figure 12 remind one of the situation found for ^{1}H, where low-field shifts were observed when the hydrogen bonds became shorter, which were maximum when H was located in the hydrogen bond center and then decreased again after full H transfer.[31,56] To our knowledge, this feature of ammonium ^{15}N chemical shifts has not yet been recognized.

In the case of the hydrochloride and hydrobromide salts, the values of r_{NH} are substantially reduced as compared to the corresponding 1:1 complexes. On the other hand, this leads to a strong deshielding of about 10 ppm in the case of the former, but only a minor chemical shift change is observed for the latter. The values of r_{NH} are similar to those of hydrated methylammonium, but again, the hydrogen bond deshielding persists. We associate this finding with the large size of the electronic system

of these halide anions and their larger number in the salt as compared to the 1:1 complexes. The ring currents produced in the electronic systems of these anions are much larger than those in the oxygen atoms and hence lead to the observed deshielding. Thus, the larger N···X distances in the halide salts as compared to the 1:1 complexes are compensated by the larger number of neighboring halide anions. If all ammonium groups could be deprotonated at the same time, keeping periodic boundary conditions, which is probably unphysical, we may expect a shielding behavior as indicated by the dashed correlation line in Figure 12a. We associate the deviations observed for acetic acid (Figure 12b) at small values of r_{NH} with the switch from a single to the above-mentioned double hydrogen bond of methylammonium with acetate.

Figure 13a shows a good correlation of the calculated chemical shifts for the isolated complexes with those found for the acid−base complexes in PLL. In particular, this correlation is in agreement with the assumption that HF and the other oxygen acids do not form alkylammonium salt structures as HCl, HBr, and HI but as hydrogen-bonded complexes which are sufficiently far away from each other for a mutual interaction and salt formation. This is supported by the finding that in the case of HF and the oxygen acids, the $^{13}C_\alpha$ and ^{13}CO signals of PLL exhibit two sharp components typical for a superposition of α-helical domains and β-sheets (Figure 6). By contrast, salt formation is associated with broad signals assigned to disordered β-sheets. We could not definitively establish the proton positions in the hydrogen-bonded complexes C.

In order to estimate the margin of error of the correlation between the distances calculated for the methylamine species and those observed experimentally for PLL, we proceeded as follows. We calculated the ^{15}N shielding values estimated for the PLL species from the solid correlation line in Figure 13a. Using these values, we estimated then the corresponding N···H and H···X distances numerically using the hydrogen bond correlation of eqs 2−5. With a larger margin of error, these distances could also be determined graphically from the correlation lines of Figures 11 and 12. The values obtained are included in the last two rows of Table 1. They deviate substantially from the ones calculated for the methylamine species assembled in the left part of Table 1 and give a feeling for the margin of error which might be involved. However, despite this variation, the estimated distances for PLL support the finding that HF and the other oxygen acids only form hydrogen-bonded complexes and not salts.

Finally, Figure 13b supports that ring currents induced in the electronic systems of the neighboring anions are responsible for the difference between the ^{15}N chemical shifts of the halide salts, which all exhibit very similar N···H distances of about 1 Å. These shifts increase with the size of the anion, as measured by the N···X distance. Note that the chemical shifts increase again if either the number of halide anions is reduced or if the nitrogen−halide distance is increased for a given halide. Thus, the hydration shift observed by dissolving $(Lys-NH_3^+Cl^-)_n$ in water arises from the replacement of the large halide anions by the small oxygen atoms of water. These results can also explain the previous findings of Hansen et al.[25] that the ammonium ^{15}N chemical shifts as well as H/D isotope effects on the latter increase when the size and the concentration of the halide anion is increased.

Conclusions

The combination of high-resolution solid-state ^{15}N NMR with DFT geometry and chemical shielding calculations has allowed us to characterize the protonation and hydrogen-bonded states of the side chain amino groups of poly-L-lysine in the presence of added acids HX. It is shown that the approach of hydrogen toward nitrogen first leads to ^{15}N deshielding, the shielding goes through a minimum when H is located in the hydrogen bond center, and then increases again in a similar way as is well established for hydrogen-bonded protons. Oxygen acids and HF lead in the dry solid only to the formation of hydrogen-bonded complexes $(Lys-NH_2\cdots H\text{-}X)_n$ in a similar way as in the gas phase. The associated increase of the H···X and decrease of the N···H distances leads to low-field ^{15}N shifts. Full protonation is only achieved in water at low pH, which leads again to a high-field shift. By contrast, stronger low-field shifts are observed for the halogen acids HCl, HBr, and HI, which form internal salt structures of the type $(Lys-NH_3^+X^-)_n$. These low-field shifts increase with the size and the number of the neighboring anions and arise hence from anisotropic deshielding of their electronic systems. Dissolving ammonium groups in water replaces the large halide anions by oxygen atoms and causes significant high-field hydration shifts.

As the polarity of dry solid PLL is expected to be small, internal salt formation requires the approach of many acid−base pairs, as has well been established for ammonia−HCl mixtures. This approach is possible only when the main chain of PLL adopts a β-sheet conformation. Thus, α-helices where the side chains are farther away from each other can only form hydrogen-bonded complexes in dry solid PLL. The absence of salt formation with HF can be explained in terms of the larger local electric fields required for the dissociation of HF, as compared to the other halogen acids.[45] A prerequisite of salt formation seems also to be the ability of the halide anions to form several hydrogen bonds into any direction of space, which allows them to adapt to the orientation of the amino side chains. By contrast, in the case of the oxygen acids, hydrogen bonds can be only formed in specific orientations which are mismatched with the amino acid side chain orientations.

Many interesting questions remain, that is, the behavior of the amino groups when they have to compete for a small number of acid molecules and the interaction with added water and with polyacids such as DNA. Moreover, more sophisticated NMR methods may be applied to further support our findings in the near future.

Acknowledgment. This work has been supported by the Deutsche Forschungsgemeinschaft and the Fonds der Chemischen Industrie, Frankfurt.

Supporting Information Available: Full ref 33 and Tables S1 and S2 containing calculated distances and ^{15}N shielding parameters of methylamine−acid complexes and of poly-L-lysine interacting with different acids used to prepare the graphs of Figures 11−13. This material is available free of charge via the Internet at http://pubs.acs.org.

References and Notes

(1) Shmueli, U.; Traub, W. *J. Mol. Biol.* **1965**, *12*, 205–214.
(2) Suwalsky, M.; Llanos, A. *Biopolymers* **1977**, *16*, 403–413.
(3) Belfiore, L. A.; McCurdie, M. P. *Pol. Eng. Sci.* **2000**, *40*, 738–746.
(4) Krushelnitsky, A.; Faizullin, D.; Reichert, D. *Biopolymers* **2004**, *73*, 1–15.
(5) Swanson, S. D.; Bryant, R. C. *Biopolymers* **1991**, *31*, 967–973.
(6) Cui, H.; Krikorian, V.; Thompson, J.; Nowak, A. P.; Deming, T. J.; Pochan, D. J. *Macromolecules* **2005**, *38*, 7371–7377.
(7) Kricheldorf, H. R.; Müller, D. *Macromolecules* **1983**, *16*, 615–623.

(8) Prestrelski, S. J.; Tedeschi, N.; Arakawa, T.; Carpenter, J. F. *Biophys. J.* **1993**, *65*, 661–671.
(9) Ma, L.; Ahmed, Z.; Mikhonin, A. V.; Asher, S. A. *J. Phys. Chem. B* **2007**, *111*, 7675–7680, and literature cited therein.
(10) Wilson, G.; Hecht, L.; Barron, L. D. *J. Chem. Soc., Faraday Trans.* **1996**, *92*, 1503–1509.
(11) Saitô, H.; Smith, I. C. P. *Arch. Biochem. Biophys.* **1973**, *158*, 154–163.
(12) Perly, B.; Chevalier, Y.; Chachaty, C. *Macromolecules* **1981**, *14*, 969–975.
(13) Davidson, B.; Fasman, G. D. *Biochemistry* **1967**, *6*, 1616–1629.
(14) Painter, P. C.; Koenig, J. L. *Biopolymers* **1976**, *15*, 229–240.
(15) Jackson, M.; Haris, P. I.; Chapman, D. *Biochim. Biophys. Acta* **1989**, *998*, 75–79.
(16) Carrier, D.; Mantsch, H.; Wong, P. T. T. *Biopolymers* **1990**, *29*, 837–844.
(17) (a) Nemethy, G.; Scheraga, H. A. *J. Phys. Chem.* **1962**, *66*, 1773–1789. (b) Scheraga, H. A. *Chem. Rev.* **1971**, *71*, 195–217. (c) Hesselink, F. T.; Ooi, T.; Scheraga, H. A. *Macromolecules* **1973**, *6*, 541–552. (d) Vorobjev, Y. N.; Scheraga, H. A.; Honig, B. *J. Phys. Chem.* **1995**, *99*, 7180–7187. (e) Vorobjev, Y. N.; Scheraga, H. A.; Hitz, B.; Honig, B. *J. Phys. Chem.* **1994**, *98*, 10940–10948.
(18) Rozenberg, M.; Shoham, G. *Biophys. Chem.* **2007**, *125*, 166–171.
(19) Hull, W. E.; Kricheldorf, H. R.; Fehrle, M. *Biopolymers* **1978**, *17*, 2427–2443.
(20) Martin G. J.; Martin M. L.; Gouesnard J.-P. *15N-NMR Spectroscopy* Springer-Verlag: Berlin, Heidelberg, New York, 1981.
(21) Schimming, V.; Hoelger, C. G.; Buntkowsky, G.; Sack, I.; Fuhrhop, J. H.; Rocchetti, S.; Limbach, H. H. *J. Am. Chem. Soc.* **1999**, *121*, 4892–4893.
(22) Maeda, S.; Mori, T.; Sasaki, C.; Kunimoto, K. K.; Kuwae, A.; Hanai, K. *Polym. Bull.* **2005**, *53*, 259–267.
(23) Angeles García, M.; López, C.; Peters, O.; Claramunt, R. M.; Klein, O.; Schagen, D.; Limbach, H. H.; Foces-Foces, C.; Elguero, J. *Magn. Reson. Chem.* **2000**, *38*, 604–614.
(24) (a) Hayashi, S.; Hayamizu, K. *Bull. Chem. Soc. Jpn.* **1991**, *64*, 688–690. (b) Witanowski, M.; Stefaniak, L.; Szymański, S.; Januszewski, H. *J. Magn. Reson.* **1977**, *28*, 217–226.
(25) (a) Hansen, P. E.; Lycka, A. *Acta Chem. Scand.* **1989**, *43*, 222–232. (b) Munch, M.; Hansen, A. E.; Hansen, P. E.; Bouman, T. D. *Acta Chem. Scand.* **1992**, *46*, 1065–1071.
(26) Zanotti, J. M.; Bellissent-Funel, M. C. *Biophys. J.* **1999**, *76*, 2390–2411.
(27) Bergmann, M.; Zervas, L.; Ross, W. F. *J. Biol. Chem.* **1935**, *111*, 245–260.
(28) (a) Neuberger, A.; Sanger, F. *Biochem. J.* **1943**, *37*, 515–518. (b) Kurtz, A. C. *J. Biol. Chem.* **1949**, *180*, 1253–1267.
(29) Fasman, G. D.; Ideslon, M.; Blout, E. R. *J. Am. Chem. Soc.* **1961**, *83*, 709–712.
(30) Hernandez, J. R.; Klok, H. A. *J. Polym. Sci., Part A: Polym. Chem.* **2003**, *41*, 1167–1186.
(31) (a) Sharif, S.; Denisov, G. S.; Toney, M. D.; Limbach, H. H. *J. Am. Chem. Soc.* **2007**, *129*, 6313–6327. (b) Sharif, S.; Schagen, D.; Toney, M. D.; Limbach, H. H. *J. Am. Chem. Soc.* **2007**, *129*, 4440–4455. (c) Sharif, S.; Chan Huot, M.; Tolstoy, P. M.; Toney, M. D.; Jonsson, K. H. M.; Limbach, H. H. *J. Phys. Chem. B* **2007**, *111*, 3869–3876.
(32) Becke, A. D. *J. Chem. Phys.* **1993**, *98*, 5648.
(33) Frisch, M. J. et al. *Gaussian 98*, revision A.11; Gaussian, Inc.,: Pittsburgh, PA, 2001; for the full reference, see Supporting Information.
(34) Perdew, J. P. *Electronic Structure of Solids*; Akademie Verlag: Berlin, Germany, 1991.
(35) Perdew, J. P.; Wang, Y. *Phys. Rev. B* **1992**, *45*, 13244–13249.
(36) Saunders, V. R.; Dovesi, R.; Roetti, C.; Orlando, R.; Zicovich-Wilson, C. M.; Harrison, N. M.; Doll, K.; Civalleri, B.; Bush, I. J.; D'Arco, P.; Llunell, M. *CRYSTAL03 User's Manual*; Università di Torino: Torino, Italy, 2003.
(37) Dovesi, R.; Causà, M.; Orlando, R.; Roetti, C. *J. Chem. Phys.* **1990**, *92*, 7402–7411.
(38) Civalleri, B.; Casassa, S.; Garrone, E.; Pisani, C.; Ugliengo, P. *J. Phys. Chem. B* **1999**, *103*, 2165–2171.
(39) Nada, R.; Catlow, C. R. A.; Pisani, C.; Orlando, R. *Modell. Simul. Mater. Sci. Eng.* **1993**, *1*, 165–187.
(40) Aprà, E.; Causà, M.; Prencipe, M.; Dovesi, R.; Saunders, V. *J. Phys.: Condens. Matter* **1993**, *5*, 2969–2976.
(41) Hay, P. J.; Wadt, W. R. *J. Chem. Phys.* **1985**, *82*, 299–310.
(42) Ugliengo, P.; Viterbo, D.; Chiari, G. *Z. Kristallogr.* **1993**, *207*, 9–23.
(43) (a) Henderson, L. J. *Am. J. Phys.* **1908**, *21*, 173–179. (b) De Levie, R. *J. Chem. Educ.* **2003**, *80*, 146–146.
(44) Sharif, S.; Shenderovich, I. G.; González, L.; Denisov, G. S.; Silverman, D. N.; Limbach, H. H. *J. Phys. Chem. B* **2007**, *111*, 6084–6093.
(45) (a) Golubev, N. S.; Denisov, G. S.; Smirnov, S. N.; Shchepkin, D. N.; Limbach, H. H. *Z. Phys. Chem.* **1996**, *196*, 73–84. (b) Ramos, M.; Alkorta, I.; Elguero, J.; Golubev, N. S.; Denisov, G. S.; Benedict, H.; Limbach, H. H. *J. Phys. Chem. A* **1997**, *101*, 9791–9800.
(46) Limbach, H. H.; Denisov, G. S.; Golubev, N. S. Hydrogen Bond Isotope Effects Studied by NMR. In *Isotope Effects in the Biological and Chemical Sciences*; Kohen, A.; Limbach, H. H. Taylor & Francis: Boca Raton, FL, 2005; Chapter 7, pp 193−230.
(47) (a) Pauling, L. *J. Am. Chem. Soc.* **1947**, *69*, 542–553. (b) Brown, I. D. *Acta Crystallogr., Sect. B* **1992**, *48*, 553–572. (c) Bürgi, H. B.; Dunitz, J. D. *Acc. Chem. Res.* **1983**, *16*, 153–161.
(48) Benedict, H.; Shenderovich, I. G.; Malkina, O. L.; Malkin, V. G.; Denisov, G. S.; Golubev, N. S.; Limbach, H. H. *J. Am. Chem. Soc.* **2000**, *122*, 1979–1988.
(49) Shenderovich, I. G.; Tolstoy, P. M.; Golubev, N. S.; Smirnov, S. N.; Denisov, G. S.; Limbach, H. H. *J. Am. Chem. Soc.* **2003**, *125*, 11710–11720.
(50) Sharif, S.; Denisov, G. S.; Toney, M. D.; Limbach, H. H. *J. Am. Chem. Soc.* **2006**, *128*, 3375–3387.
(51) Limbach, H. H.; Pietrzak, M.; Benedict, H.; Tolstoy, P. M.; Golubev, N. S.; Denisov, G. S. *J. Mol. Struct.* **2004**, *706*, 115–119.
(52) Limbach, H. H.; Pietrzak, M.; Sharif, S.; Tolstoy, P. M.; Shenderovich, I. G.; Smirnov, S. N.; Golubev, N. S.; Denisov, G. S. *Chem.−Eur. J.* **2004**, *10*, 5195–5204.
(53) Satyanarayana, Ch. *Phys. Rev. B* **1984**, *30*, 1004–1007.
(54) Lorente, P.; Shenderovich, I. G.; Golubev, N. S.; Denisov, G. S.; Buntkowsky, G.; Limbach, H. H. *Magn. Reson. Chem.* **2001**, *39*, 18–29.
(55) Lopez, J. M.; Männle, F.; Wawer, I.; Buntkowsky, G.; Limbach, H. H. *Phys. Chem. Chem. Phys.* **2007**, *9*, 4498–4513.
(56) Wright, D. A.; Marsh, R. E. *Acta Crystallogr.* **1962**, *15*, 54–64.

JP806551U